



OPEN

Ce(III) and La(III) ions adsorption through Amberlite XAD-7 resin impregnated via CYANEX-272 extractant

Azadeh Yarahmadi¹, Mohammad Hassan Khani^{2✉}, Masoud Nasiri Zarandi¹ & Younes amini^{2✉}

The goal of this paper is to investigate the ability of Amberlite XAD-7 (AXAD-7) resin impregnated with CYANEX-272 (di-2,4,4-trimethylpentyl phosphonic acid) to remove cerium (Ce(III)) and lanthanum (La(III)) ions from aqueous solutions in the batch scheme. The prepared adsorbent material was determined utilizing FTIR, SEM-EDX, and BET methods. The impact of three individual process variable factors involving feed solution pH (2–6), adsorbent dose (0.05–0.65), and process temperature (15–55 °C) on the simultaneous removal of Ce(III) and La(III) ions was evaluated via response surface methodology (RSM) according to the central composite design (CCD). The modeling of Ce(III) and La(III) ions adsorption was performed using the quadratic model and was evaluated using a coefficient of determination for both ions. The optimization data revealed that the adsorption amount of Ce(III) and La(III) ions removal under optimal conditions were 99.75% and 69.98%, respectively. Equilibrium and kinetic investigations were also conducted to define the removal performance of the calculated adsorbent for Ce(III) and La(III) ions removal. Various isotherms models such as Langmuir, Freundlich, Temkin, and Sips were examined at 25 °C to analyze the equilibrium isotherm data. The data revealed that the Sips approach is compatible with the experimental data. The highest adsorption capacity of the resin for Ce(III) and La(III) ions were 11.873 mg g⁻¹ and 7.324 mg g⁻¹, correspondingly. The kinetic study of the Ce(III) and La(III) adsorption process was conducted via pseudo-first-order, pseudo-second-order, and intraparticle diffusion models (IDMs). Based on the data obtained, kinetic data were fitted well to a pseudo-second-order rate correlation. According to the obtained results, the (AXAD-7) resin impregnated with CYANEX-272 performed well in removing both Ce(III) and La(III) ions from aqueous solutions with well stability during several adsorption–desorption cycles and well regeneration and excellent metallic ions recovery.

Rare earth elements (REE), which are in the category of industrial, chemical, and precious metals, contain 15 elements of lanthanides from lanthanum(57) to lutetium(71) and the two components of yttrium (39) and scandium (21)^{1–4}. (REE) have similar physical and chemical properties due to their stable trivalent ions of the same size. The unique properties of these elements have caused them to be widely used in various industries in recent decades, such as the nuclear industry, ceramic, and glass production^{5–8}, petrochemical and catalytic industry^{9,10}, electronics and metallurgy, etc.^{11,12}. Amongst the REE, cerium (Ce) and lanthanum (La) have received growing interest recently, due to their high technological applications^{13–16}.

Due to the wide applications of these Rare earth elements in new industries, key technologies, and their commercial importance, their demand is remarkably increased¹⁷. There is a high probability that a significant amount of the cerium and lanthanum elements will enter the environment during their separation and purification process. These elements collect in the human body when inhaled or digested from the food chain and could generate several problems for human health¹⁸. Common approaches for the elimination of REE from aqueous solutions involve reverse osmosis, solvent extraction¹⁹, chemical deposition, ion exchange, adsorption, etc.²⁰. Among these various methods, the adsorption process using solvent-impregnated resins (SIR) demonstrated an efficient, effective, and economical technology²¹. In this method, the surface of the resin

¹Department of Chemical Engineering, Faculty of Oil and Gas Engineering, Semnan University, P.O.BOX: 35131-1911, Semnan, Iran. ²Nuclear Fuel Cycle Research School, Nuclear Science and Technology Research Institute, P.O.BOX: 11365-8486, Tehran, Iran. ✉email: mhkhani@aeoi.org.ir; Y_amin@alum.sharif.edu; Yamini@aeoi.org.ir

is impregnated with a chelating solvent, usually containing the organic compounds of the cavity, and the ion exchange process is performed by it²². SIRs have the properties of ion exchange resins and solvent extraction methods simultaneously^{19,23}. Compared to other separation methods, this technology has advantages such as simple design, more flexibility, suitable physical and chemical stability, production of minimal secondary residues, and the possibility of resin recovery²⁴. Resin surface properties and extractant functional groups are important in SIR efficiency and the adsorption process²⁵. XAD series microporous resins are one of the most important resins in the preparation of SIR and as a neutral polymer base; having a strong structure with a highly effective level to provide the best substrate for SIR²⁶. So far the adsorption of many metals such as Cu(II), Fe(II), Pb(II), Cd(II), Zn(II), Bi(III), and Co(II) has been successfully performed using SIRs by the selection of suitable extractant²⁷. The possibility of using hydrogenated Dowex 50WX8 resin for the recovery and separation of Pr(III), Dy(III) and Y(III) from aqueous nitrate solutions were carried out by Masry and coworkers and promising results were obtained in determined optimal operating conditions²⁸.

The results of other reported works for the uses of SIR with different inert resin with other extractants have appeared promising in the absorption and separation of metals. TVEX-TOPO, which is a commercial low-cost macroporous copolymer resin containing 50% (w/w Extractant fraction of total adsorbent mass) trioctylphosphine oxide (TOPO) was used for solid-liquid extraction of tungsten(VI) (W(VI)) and molybdenum(VI) (Mo(VI)) from nitric acid²⁹. Sorption of molybdenum (VI) from nitric acid solution by solvent impregnated resin (SIR) technique using bio-beads styrene divinyl benzene copolymer (SM-4) impregnated with tri-alkyl phosphine oxide (CYANEX 923 or CY 923) extractant in both batch and column systems was studied and the obtained results indicate the selectivity of the technique for molybdenum recovery from nitric acid solution³⁰.

The extraction of Pb(II) nitrate solution by (AXAD-7) resin impregnated with organophosphorus extractants (DEHPA, IONQUEST, CYANEX-272) was investigated by Draa et al.³¹. The data revealed that with improving the pH of the aqueous solution, the sorption efficiency of metal ions increases. The highest sorption efficiencies of Pb(II) ions using DEHPA and IONQUEST extractants are 95% in the pH range of 2.75–3 and 3.5–3.75, correspondingly.

El-Sofany³² evaluated the removal of La(III) and Ga(III) from nitrate medium by (AXAD-7) resin impregnated via Aliquat-334 extractant. According to their reports, the experimental adsorption data for La(III) and Ga(III) fit better with the Freundlich isotherm, and the highest adsorption capacity for La(III) and Ga(III) using impregnated resin is 4.73 and 4.4 mg/g, respectively.

Belkholuch and Didi³³ investigated the removal of Bi(III) ions from aqueous nitrate solution through AXAD-1180 impregnated with D2EHPA. Based on the obtained results, the equilibrium condition for bismuth ions adsorption is attained after 30 min. The maximum extraction yield (98.5%) of bismuth ions from mixture with the primary concentration of 250 mg/L at pH 3.6 was obtained using 15 mmol/g SIR.

Fouad et al.³⁴ employed alizarin red S-impregnated XAD-2010 as an adsorbent for pre-concentration and separation of uranium and thorium in their bearing rocks. They reported the highest adsorption amount of 18.25 mg/g and 20.2 mg/g for Th(IV) and U(VI) ions, correspondingly. According to the Langmuir model, alizarin red S-impregnated XAD-2010 is considered an effective adsorbent for U(VI) and Th(IV) recovery.

Liao et al.³⁵ examined the removal mechanism of heavy rare earth elements from hydrochloric acid solution by CYANEX-272-p507 impregnated resin. According to the results, the molar ratio of Cyanex-272-P507 to HREE (heavy rare earth elements) in the extraction complex is 3.

Kinetic studies of the divalent cadmium ions extraction with impregnated resins organized by adsorption of di(2-ethylhexyl) phosphoric acid onto macro-porous polymeric support of (AXAD-7) resin were performed by Benamor et al.³⁶ using the homogenous diffusion model. According to the obtained results, a cadmium diffusion coefficient of about 10^{-12} m²/s was predicted in the range of investigated parameters.

Chen et al.³⁷ investigated the optional separation of Vanadium from Molybdenum ions via the impregnation technique including blends of organophosphorus extractant (DEHPA) complexes stabled onto AXAD-4. The findings of this study revealed that the D2EHPA- Immobilized AXAD -4 resin adsorbs Molybdenum ions higher than Vanadium ions, and the best separation of these ions occurs at pH 6.

The Adsorption of U(VI) ions from Egyptian crude phosphoric acid through a batch experiment method using AXAD -2 resin fertilized with tri-butyl phosphate (TBP) and di-2-ethylhexyl phosphoric acid (D2EHPA) as adsorbent was studied³⁸. In the current work, the highest sorption capacity of 67 mg/g was obtained for the adsorption of U(VI) ions on improved AXAD-2 resin. The data showed that the modified resin is an efficient adsorbent for U (VI) elimination from Egyptian crude phosphoric acid.

Sett et al.²² investigated the sorption performance of a group of rare earth elements on DEHPA-impregnated XAD-7 resin in a nitric acid medium. They stated that the adsorption process of rare earth elements reaches equilibrium after 120 min, and the Pseudo-Second-Order kinetic scheme is compatible with the experimental result.

Equilibrium and kinetics for the adsorption Biphenol-A from aqueous solutions with AXAD-7 resin containing Aliquat-336 have been studied in batch and column experiments by Betra et al.³⁹. They assumed that the adsorbent with 1 g of Aliquat-336 per g of A XAD-7 was able to remove 88.98% of Biphenol-A from aqueous solutions. Also, the used IX7-1 resin was recovered 5 times and showed high stability during 5 adsorption-desorption cycles.

Moreover, a di(2-ethylhexyle) phosphoric acid (D2EHPA) fertilized XAD-4 resin is produced and its adsorption-desorption performance was investigated for uptake of Sr(II) ions in aqueous solutions⁴⁰. According to the obtained results, the percentage adsorption of strontium ions onto the impregnated XAD-4 resin at optimal pH was 94.0%.

The literature review indicates that SIRs are efficiently employed for the extraction of metal ions in analytical and environmental applications. Easy handling, quick operation, high loading capacity as well as stability during

several adsorption–desorption cycles, make this approach an efficient, economical, and promising technology for metal ions removal^{41–45}.

The current work investigated the ability of AXAD-7 resin impregnated with CYANEX-272 (SIR) for Ce(III) and La(III) ions adsorption from aqueous solutions. The adsorption process modeling was performed using RSM according to CCD to assess the impact of pH of the metal ion solution, SIR dose, and temperature on Ce(III) and La(III) ions percentage adsorption. The sorption of Ce(III) and La(III) ions onto SIR also was assessed according to the equilibrium and kinetics. The isotherm approaches such as Langmuir, Freundlich, Temkin, and Sips were utilized to explain the equilibrium result. The kinetic result achieved from the batch sorption runs has been matched by pseudo-first-order, second-order correlations, and (IDMs).

Materials and method

Chemicals and tools. CYANEX-272 (di-2,4,4-trimethylpentylphosphinic acid), toluene (C₆H₅CH₃), sodium hydroxide (NaOH), nitric acid (HNO₃), lanthanum nitrate (La(NO₃)₃·6H₂O), cerium nitrate (Ce(NO₃)₃·H₂O) salts were of fluka products. Amberlite XAD-7 was prepared from Merck. All chemicals applied in this study were of analytical grade.

Ce(III) and La(III) ions measurements were done using PerkinElmer Optima 2000 DV Inductivity coupled plasma device atomic emission spectrometer (ICP-AES). The batch sorption tests were accomplished via a thermostatic shaking water bath GFL-1083 Model. A pH meter is used to calculate the solution pH (Metrohm 780 Model).

To characterize the prepared SIR, the fourier transform infrared (FTIR) spectrometer (Vector22-Bruker Company, Germany) at wavenumbers between 400 and 4000 cm⁻¹ was used to recognize the resin functional groups. Specific surface area, pore size distribution, and microporosity of SIR have been specified by Brunauer–Emmett–Teller (BET) analysis using nitrogen as carrier gas at 77 K (Quantachrome Autosorb-1 model). The scanning electron microscope (SEM) combined with Energy Dispersive X-ray (EDX) using a TESCAN Vega TS 5136LM generally at acceleration voltage 20 kV, was employed to determine morphology and elemental constituents of prepared SIR.

Preparation of the SIR. Before fertilization, the AXAD-7 resin was rinsed various times via distilled water to eliminate contaminations and then dehydrated at room temperature (25 °C ± 1).

The SIR was prepared by dry method; the impregnation solution was produced by mixing 0.87 g of CYANEX-272 in 30 ml toluene and mixed with 15 g of AXAD-7 resin. The resulting slurry was gently agitated for 3 h and then, the SIR was mixed with 0.1 mol L⁻¹ Hydrochloric acid and dried at ambient room temperature (25 °C ± 1) for 48 h.

RSM experimental plan. In the present study, CCD is employed to calculate the main interaction of 3 individual parameters including the primary solution pH (A), temperature (B), and SIR dose (C), on the adsorption of Ce(III) and La(III) aqueous solutions. In CCD, five levels are considered for each independent parameter, which includes a central point and two factorial points that are ± 1 unit away from the central point. There are also two-star points that make it possible to estimate the curvature and are ± α until away from the center point. Table 1 provided the coded and actual values of the independent factors.

To investigate the percentage adsorption of Ce(III) and La(III) ions onto A XAD-7 resin fertilized with CYANEX-272, 20 experiments containing six duplicates at the midpoints (to assess the pure error) were performed. The experimental plan network is presented in Table 2.

The output responses of Ce(III) and La(III) ions' percentage adsorption can be predicted using the quadratic model according to Eq. (1).

$$Y = \beta_0 + \sum \beta_i x_i + \sum \beta_{ii} x_i^2 + \sum \sum \beta_{ij} x_i x_j \quad (1)$$

The above formula shows the predicted response with Y and the coefficients of the equation with β_{ij} , β_{ii} , β_i , β_0 and the independent variables with X_i and X_j ($i \neq j$). Independent variables are used in calculations in the form of coded rolling. The reliability of this model was explained based on the coefficients of determination (R²), and its adequacy was extra calculated by analysis of variance (ANOVA) and lack-of-fit test^{46–54}.

Batch adsorption experiments. Simultaneous adsorption of Ce(III) and La(III) ions in the batch system was studied according to pH, SIR dose, and process temperature according to the experimental design matrix (Table 2). To perform adsorption experiments, the first 20 ml of a solution containing Ce(III) and La(III) ions with a specified concentration was poured into 100 ml polyethylene containers and the pH of the solution was

Variable	Symbols	Levels				
		−α = −2	−1	0	+1	+α = +2
pH	A	2	3	4	5	6
Temperature (°C)	B	15	25	35	45	55
SIR dose (gr)	C	0.05	0.2	0.35	0.5	0.65

Table 1. Coded and actual levels of the independent parameters in CCD (α = axial points).

Run order	Independent variables			Adsorption (%)			
	Initial pH	Sorption Temperature (°C)	SIR dose (g)	Ce(III)		La(III)	
				Experimental	Predicted	Experimental	Predicted
1	5	25	0.5	98.99	97.50	73.16	68.35
2	5	45	0.2	47.11	48.54	30.39	30.54
3	3	45	0.2	37.93	36.40	19.71	19.75
4	4	35	0.35	74.23	72.42	43.57	43.96
5	5	25	0.2	47.48	45.96	27.03	28.03
6	4	15	0.35	71.82	71.87	45.05	41.38
7	4	35	0.35	74.30	72.42	43.64	43.96
8	5	45	0.5	99.54	98.07	71.38	71.07
9	4	35	0.35	73.91	72.42	43.84	43.96
10	3	45	0.5	96.93	96.40	58.71	59.46
11	2	35	0.35	67.03	66.79	32.47	32.45
12	4	35	0.05	11.19	10.64	7.47	7.55
13	4	55	0.35	76.32	75.80	46.02	46.57
14	4	35	0.35	74.17	72.42	43.56	43.96
15	3	25	0.2	35.56	34.02	17.57	17.78
16	4	35	0.65	99.90	102.87	87.18	80.78
17	6	35	0.35	86.34	84.72	55.05	56.16
18	4	35	0.35	74.25	72.42	43.37	43.96
19	3	25	0.5	92.04	95.59	62.02	57.03
20	4	35	0.35	73.81	72.42	43.79	43.96

Table 2. Experimental plan network and average calculated percentage adsorption of Ce(III) and La(III) ions.

regulated via nitric (HNO₃) acid and (NaOH) of 0.1 M. Then a certain amount of resin was introduced to the mixture and the polyethylene containers were located in a shaker for 180 min at a certain temperature. After the desired time, the resins were isolated from the mixture through filter paper, and the equilibrium concentration of Ce(III) and La(III) ions in the solution was measured by ICP-AES. All tests were repeated twice and mean values were reported.

The adsorption capacity (q) of Ce(III) and La(III) per unit mass of resin (mg g⁻¹) and the percentage adsorption of these metal ions from aqueous mixture were measured via Eqs. (2) and (3), respectively.

$$q = (c_i - c_e) \times \frac{V}{M} \quad (2)$$

$$\% \text{Adsorption} = \frac{c_i - c_e}{c_i} \times 100 \quad (3)$$

In the above equations, C_i (mg L⁻¹) and C_e (mg L⁻¹) are the primary concentration and equilibrium concentration of metal ions in the solution, respectively⁵⁵. The weight of the dry adsorbent is also denoted by M (g) and the volume of the solution by V (L).

Adsorption/desorption studies. One of the important factors in selecting the adsorbent is the ability of the adsorbent to recover. If it is not possible to recover the adsorbent after the adsorption process, the adsorbent itself is a biological contaminant. To create the highest amount of adsorption/desorption cycles of Ce(III) and La(III) ions were adsorbed and desorbed till the adsorption is not anymore achievable. For this purpose, desorption was performed by mixing 1 g of the SIR involving adsorbed ions with 10 mL of 2 mol L⁻¹ HCl mixture. The mixture was agitated for 24 h at 150 rpm at 25 C. Then, the SIR was isolated via filter paper and washed with purified water, and dehydrated at ambient conditions. This stage was duplicated till the Ce(III) and La(III) ions are irretrievably mounted to the adsorbent material shell, setting up the plan for the highest quantity of usage cycles.

Results and discussion

Characterization of the SIR. *Infrared spectra analysis.* FTIR spectra of AXAD-7 resin, CYANEX-272 fertilized resin, and Ce(III) and La(III) loaded resin was shown in Fig. 1a,b,c, correspondingly. As can be observed the band located in the limited area of 3500–3000 cm⁻¹ is attributed to the presence of O–H bonds and is due to the presence of moisture in the Amberlite XAD-7 resin. After resin impregnation, the peak attributed to O–H bonds is lost, which is due to the disappearance of the hydrophilic nature of the SIR^{22,39}.

The existence of the peaks placed at 2972 cm⁻¹ could be accompanied with the stretching vibration of the aliphatic C–H group. The peak around 1728 cm⁻¹ is attributed to C=O vibration which is present in both pure

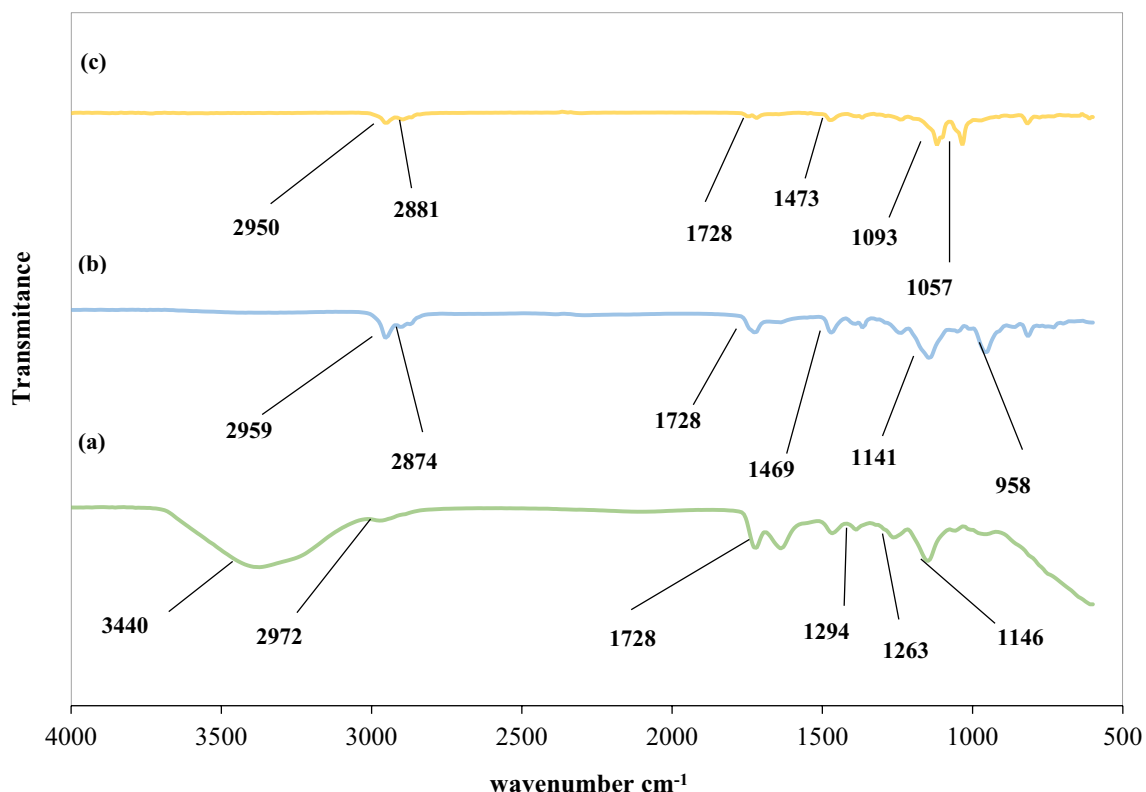


Figure 1. FTIR spectra of the working polymeric resin: (a) A XAD-7; (b) Amberlite XAD-7 resin impregnated with CYANEX-272; (c) AXAD-7 resin impregnated with CYANEX-272 after Ce(III) and La(III) adsorption.

and impregnated XAD-7 resins. The C–O stretching in the ester group can be observed near 1146 cm^{-1} and 1294 cm^{-1} location.

The peak located at 1469 cm^{-1} is attributed to the C–H deformation of the CH_3 group observed in both pure and impregnated XAD-7 resins⁵⁶.

As shown in Fig. 1b the IR peaks about 2874 cm^{-1} and 2959 cm^{-1} are corresponding to CH_2 . The presence of P=O and P–O–H stretching vibration bonds located at 958 cm^{-1} and 1141 cm^{-1} can certify the successful impregnation of XAD-7 resin with organophosphorus acid-specific groups⁵⁷. After Ce(III) and La(III) adsorption, the intensity of specific peaks has reduced and subtle shifts in the wavenumber of many bands can be observed.

SEM–EDX analysis. The SEM analysis was performed to identify the shape and morphology of the outer surface of the XAD-7 resin before and after impregnation with CYANEX-272 extractant (Fig. 2). As can be observed, the pure XAD-7 resin is transparent, but it becomes cloudy after impregnation. This color change indicates the successful performance of the resin impregnation. As shown in Fig. 2b, changes also have been made on the

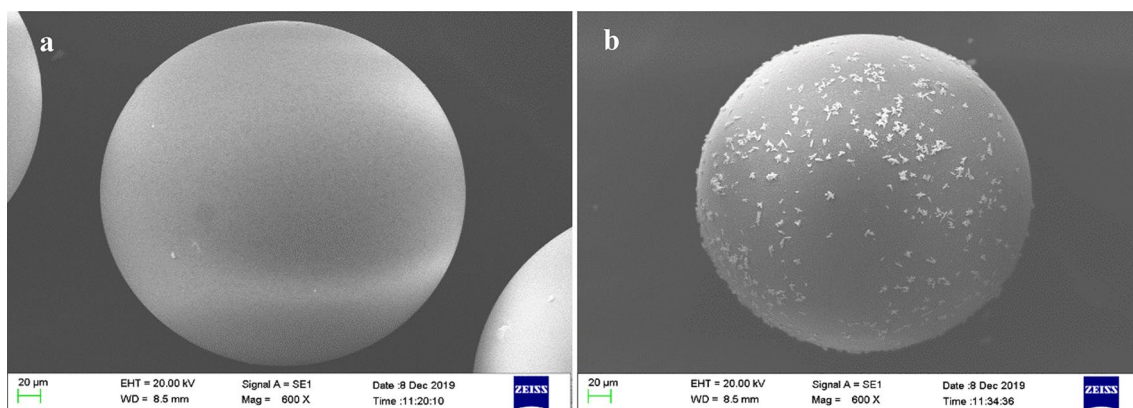


Figure 2. SEM image of A XAD-7 resin surface before (a) and after (b) impregnation with CYANEX-272.

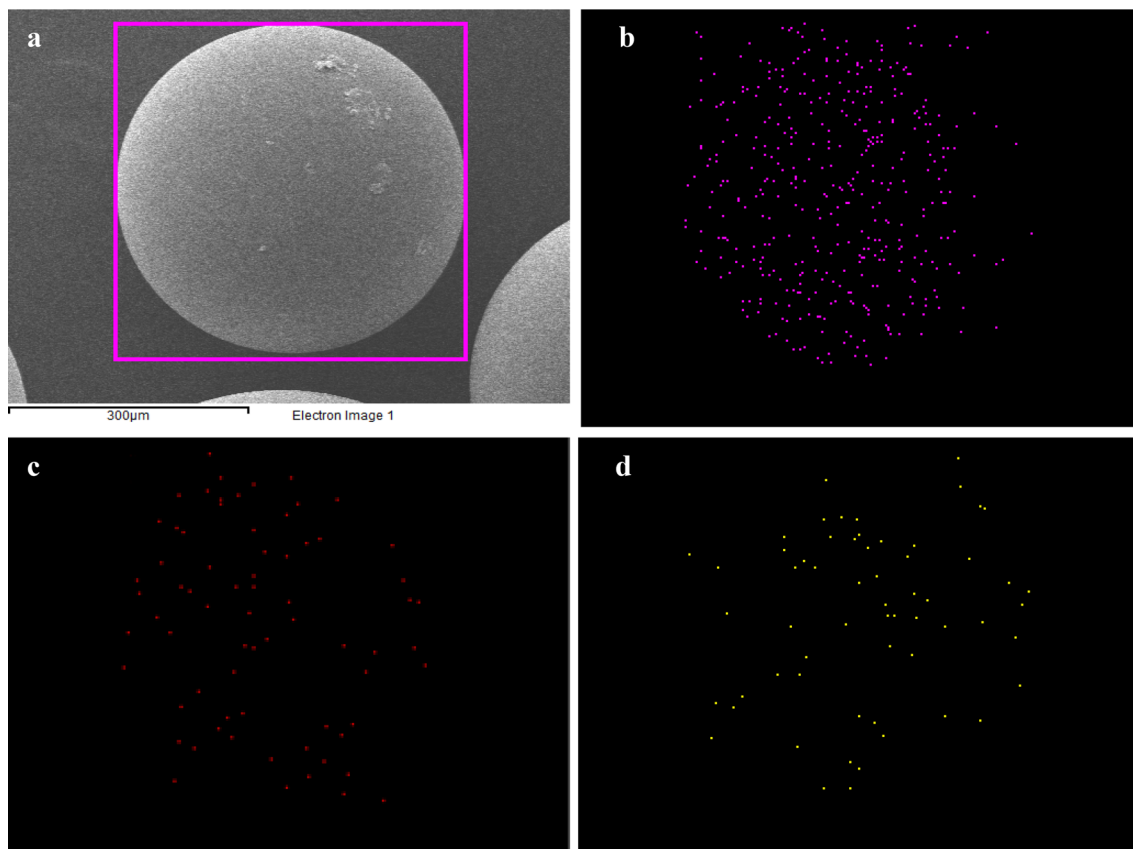


Figure 3. SEM pictures of the loaded SIR (a) and corresponding p (b), La (c) and Ce (d) elemental mappings.

outer surface of the resin after impregnation that affects the morphology of the resin. The presence of these micro granules fixed on the surface of XAD-7 resin indicates that it is functionalized by the CYANEX-272 extractant.

The SEM images of the SIR after Ce(III) and La(III) adsorption and corresponding p, La, and Ce elemental mappings are presented in Fig. 3. As observed a large amount of phosphorus was diffused on the surface of XAD-7 resin after impregnation with CYANEX-272 extractant. The homogeneous distribution of La and Ce ions on the SIR surface confirms their successful adsorption by impregnated XAD-7 resin²².

The EDX image of the XAD-7 resin impregnated with CYANEX-272 after Ce(III) and La(III) adsorption is shown in Fig. 4. According to Fig. 4, the existence of the phosphorus (P) peak denotes the successful impregnation of the resin by the CYANEX-272 extractant. Also, the presence of Ce(III) and La(III) peaks indicates their uptake by the resin.

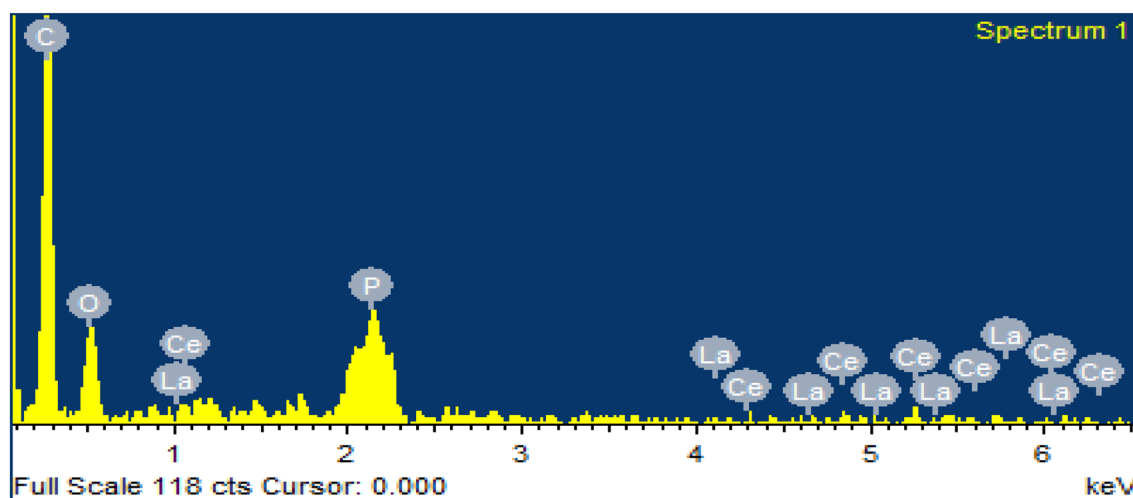


Figure 4. EDX image of SIR after Ce(III) and La(III) ions adsorption.

Resin	BET surface area (m ² /g)	BJH Adsorption average pore volume (cm ³ g ⁻¹)	Adsorption Pore Diameter (Å)
Amberlite XAD-7	450	1.14	85.63
Amberlite XAD-7 + CYANEX-272	67.16	0.57	154.13

Table 3. Surface properties of Amberlite XAD-7 and CYANEX-272 impregnated Amberlite XAD-7.

BET analysis. Table 3 presented the results of surface area and porosity analysis of A XAD-7 resin before and after impregnation with CYANEX-272. XAD-7 resin size 0.3–0.85 mm was used as support. According to the obtained results, BET Surface area and BJH adsorption average pore volume of Amberlite XAD-7 resin decreases after the impregnation process, which is due to the filling of the resin pores by CYANEX-272 organic molecules. In addition, the increase in the pore diameter of SIR indicates that in the impregnation process, first the smaller pores and then the larger pores are filled with CYANEX-272 organic molecules. The surface area and porosity analysis showed the successful saturation of the Amberlite XAD-7 resin by CYANEX-272²².

Preliminary evaluation of the impregnation process. Preliminary experiments performed for the adsorption of Ce(III) and La(III) using pure Amberlite XAD-7 resin showed that the Ce(III) and La(III) percentage adsorption on the XAD-7 resin is very low. To investigate the impact of the impregnation process on the XAD-7 resin adsorption rate, Ce(III) and La(III) adsorption tests were performed using SIR. According to the results presented in Table 4, the percentage adsorption of Ce(III) and La(III) on SIR was significantly increased and this indicates the positive effect of CYANEX-272 impregnation on XAD-7 resin ability for Ce(III) and La(III) ions adsorption.

Resin	Ce(III) Adsorption (%)	La(III) Adsorption (%)
Amberlite XAD-7	25.75	21.93
Amberlite XAD-7 + CYANEX-272	95.41	67.14

Table 4. Investigating the role of CYANEX-272 impregnation on the adsorption process (Adsorption conditions: [Ce -La] = 200 mg/L, pH = 5, resin dose = 0.4 g, agitation time: 24 h, Temperature: 25 °C).

Source	Ce(III)					La(III)				
	Sum of squares	DF	Mean of squares	F-value	P-value	Sum of squares	DF	Mean of squares	F-value	P-value
Model	54.94	9	6.10	414.80	<0.0001	43.43	9	4.83	12,592.06	<0.0001
A:pH	1.06	1	1.06	72.30	<0.0001	3.23	1	3.23	8433.92	<0.0001
B:Temperature	0.0526	1	0.0526	3.57	0.0880	0.1530	1	0.1530	399.27	<0.0001
C:SIR dose	47.56	1	47.56	3231.46	<0.0001	39.00	1	39.00	1.02E+05	<0.0001
AB	0.0001	1	0.0001	0.0056	0.9418	6.43E-06	1	6.43E-06	0.0168	0.8995
AC	0.3609	1	0.3609	24.52	0.0006	0.0658	1	0.0658	171.74	<0.0001
BC	0.0127	1	0.0127	0.8619	0.3751	0.0024	1	0.0024	6.25	0.0315
A ²	0.0500	1	0.0500	3.40	0.0952	0.0019	1	0.0019	4.96	0.0501
B ²	0.0106	1	0.0106	0.7190	0.4163	3.31E-06	1	3.31E-06	0.0086	0.9278
C ²	5.13	1	5.13	348.88	<0.0001	0.9125	1	0.9125	2381.32	<0.0001
Residual	0.1472	10	0.0147			0.0038	10	0.0004		
Lack of Fit	0.1227	5	0.0245	5.02	0.0506	0.0031	5	0.0006	4.32	0.0671
Pure Error	0.0245	5	0.0049			0.0007	5	0.0001		
Cor Total	55.09	19				43.43	19			
	R ²		0.9973			0.9999				
	R ² _{Adj}		0.9949			0.9998				
	R ² _{pred}		0.9815			0.9994				
	Adeq.precision		80.3922			451.1744				
	C.V %		1.48			0.3025				

Table 5. ANOVA for quadratic model parameters.

Statistical analysis. The process of Ce(III) and La(III) adsorption on SIR was improved via RSM according to CCD. For this purpose, 20 designed experiments were accomplished and the results are presented in Table 2. The (ANOVA) was conducted to evaluate the Ce(III) and La(III) percentage adsorption (Table 5).

According to statistical analysis, the quadratic polynomial model with square root transform function was recommended to evaluate the investigated responses and recommended models for Ce(III) and La(III) ions percentage adsorption are presented in Eqs. (4) and (5), respectively.

$$\begin{aligned} \text{Sqrt}(\% \text{Ad Ce}) = & 8.51 + 0.2579 A + 0.0573 B + 1.72 C - 0.0032 AB - 0.2124 AC - 0.0398 BC \\ & + 0.0446 A^2 + 0.0205 B^2 - 0.4519 C^2 \end{aligned} \quad (4)$$

$$\begin{aligned} \text{Sqrt}(\% \text{Ad La}) = & 6.63 + 0.4494 A + 0.0978 B + 1.56 C + 0.0009 AB - 0.0907 AC - 0.0173 BC \\ & - 0.0087 A^2 - 0.0004 B^2 - 0.1905 C^2 \end{aligned} \quad (5)$$

The mean squares are the result of dividing the total squares by the degree of freedom. The proportion of the mean squares of the results to the (MSE) represents the F-value index, which indicates the impact of each variable and their influences on the results. Its large size indicates the high impact of that variable on the response. The *p*-value index is applied to define the significance threshold of the four variables. Due to the 95% confidence interval, the importance of the variables per *p*-value is 0.05. As seen in Table 5, the F-values 414.80 and 12,592.06 for Ce(III) and La(III) accompanied by low probability quantities ($P < 0.0001$) show that the suggested patterns are considerable.

According to the ANOVA results R^2 (coefficient of determination) were 0.997 and 0.999 for Ce(III) and La(III) adsorption models, respectively. In addition, R^2_{Adj} (Adjusted R^2) for Ce(III) and La(III) was equal to 0.995, which is close to 0.999, indicating the high accuracy of the model and it indicates that the model can make a good correlation between variables and the response.

Moreover, the signal-to-noise proportion described by the satisfactory accuracy were 80.39 and 451.17 for Ce(III) and La(III), respectively; The values of more than 4 for both elements indicates an adequate signal. The amount of data distribution relative to the mean is shown using the coefficient of variation (C.V %). Due to the C.V % values less than 10 for Ce(III) (1.48) and La(III) (0.3025), the obtained models have good accuracy^{58–62}.

The calculated F-values, *p*-values, (R^2), and adjusted R^2 (adj R^2) are presented in Table 5. The data suggested that the recommended models were appropriate for the prediction of Ce(III) and La(III) ions percentage adsorption which is confirmed by a figure of estimated data versus experimental ones of Ce(III) and La(III) ions adsorption presented in Fig. 5⁶³.

Perturbation plot for Ce(III) and La(III) ions adsorption models are presented in Fig. 6. As seen from this curve, the primary pH of the mixture (factor A), Temperature (factor B), and SIR dose (factor C) have a positive impact on Ce(III) and La(III) ions adsorption. According to the perturbation plot, the SIR dose was defined as the most effective parameter on Ce(III) and La(III) ions adsorption.

Investigating the effects of process variables. To investigate the impact of independent factors and their relations on the investigated responses obtained by the polynomial models, 3D surface plots were prepared. 3D graphs show the superficial response of the performance of the two individual factors at the center part of the other individual variable on the percentage adsorption of Ce(III) and La(III) on the SIR.

Figure 7 represents the 3D plot, that illustrates the incorporated effect of temperature and SIR dose on the percentage adsorption of Ce(III) and La(III) at fixed pH of 4.

As can be seen from the graph, SIR dose significantly affects the percentage adsorption of Ce(III) and La(III) while with increasing temperature, the percentage adsorption of Ce(III) and La(III) ions slightly increases. By growing the SIR dose from 0.05 to 0.65 g at 35 °C, the percentage adsorption of Ce(III) ions was increased from 11.19 to 99.90 and the percentage adsorption of La(III) ions was increased from 7.47 to 87.18, respectively. This corresponds to the increment of the available adsorption sites for Ce(III) and La(III) ions.

The contemporaneous impact of primary mixture pH and temperature on the adsorption ratio of Ce(III) and La(III) using 0.35 g SIR is shown in Fig. 8.

As can be observed the impact of mixture pH on the adsorption percentage is greater than the temperature. By improving the primary solution pH from 2 to 6 at 35 °C, the percentage adsorption of Ce(III) ions was increased from 67.03 to 86.34 and the percentage adsorption of La(III) ions was increased from 32.47 to 55.05, respectively. Since the CYANEX-272 extractant used for impregnation of the resin is an acidic extractant and releases H^+ during the adsorption process, at low pH H^+ is more successful in competing with Ce(III) and La(III) cations in forming a complex with CYANEX-272 and the adsorption of Ce(III) and La(III) is low. With intensifying pH (decreasing the concentration of H_2 ions)³², the amount of Ce(III) and La(III) ions adsorption improved and the highest adsorption occurs at pH 6. In this method, the surface of the resin is impregnated with a chelating solvent, usually containing the organic compounds of the cavity, and the ion exchange process is performed. Similar results have been obtained from other studies for the ion exchange mechanism in using impregnated Amberlite XAD7HP resin for the removal of Cd^{2+} , Ni^{2+} , Cu^{2+} , and Pb^{2+} from aqueous solutions⁶⁴. SIRs have the properties of ion exchange resins and solvent extraction methods simultaneously^{19,23}.

Figure 9 illustrates the combined impacts of primary mixture pH and SIR dose on Ce(III) and La(III) ions adsorption. According to the obtained results, the SIR dose has a greater effect on the percentage absorption of Ce(III) and La(III) ions than the primary solution pH. Investigation of the Ce(III) and La(III) ions adsorption process using SIR showed that the impact of SIR dose on the metal ions sorption is more than the two other independent variables (pH and temperature). The maximum percentage adsorption of Ce(III) (100%) and La(III) (97%) was achieved at pH of 6, SIR dose of 0.65 g and 35 °C.

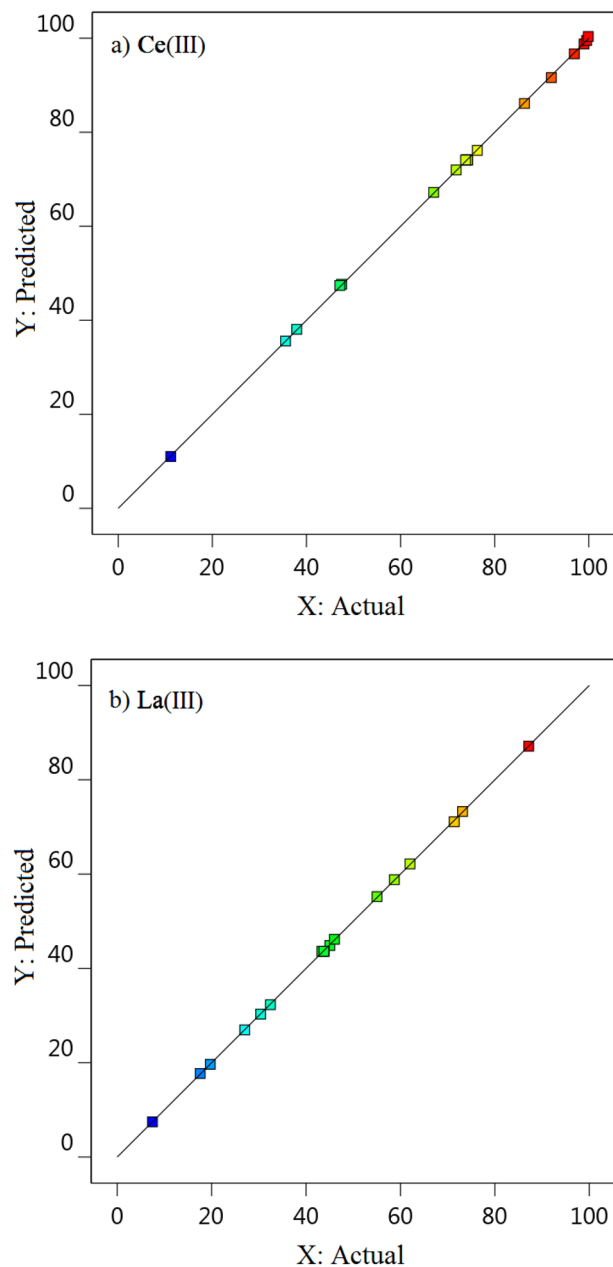
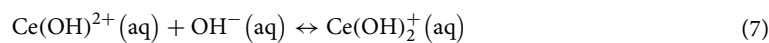
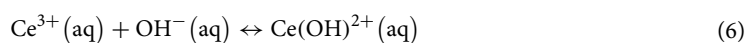


Figure 5. The sketch of calculated data versus experimental amounts of Ce(III) and La(III) ions adsorption.

According to Borai and coworkers, the normal Cerium precipitation process is highly dependent on the solution pH. This could be interpreted based on the following three equations that demonstrate the successive hydrolysis of Ce(III) in solution:



The obtained results showed that by further addition of OH^{-} , the pH rises and Ce(III) precipitates out of solution after pH 7 as a cloudy white gellike precipitate, which is presumably $\text{Ce}(\text{OH})_3(\text{s})$ ^{65,66}. Regarding lanthanum, due to the fact that there is a possibility of precipitation in alkaline pHs⁶⁷, therefore, the studied pH range was limited to acidic pHs.

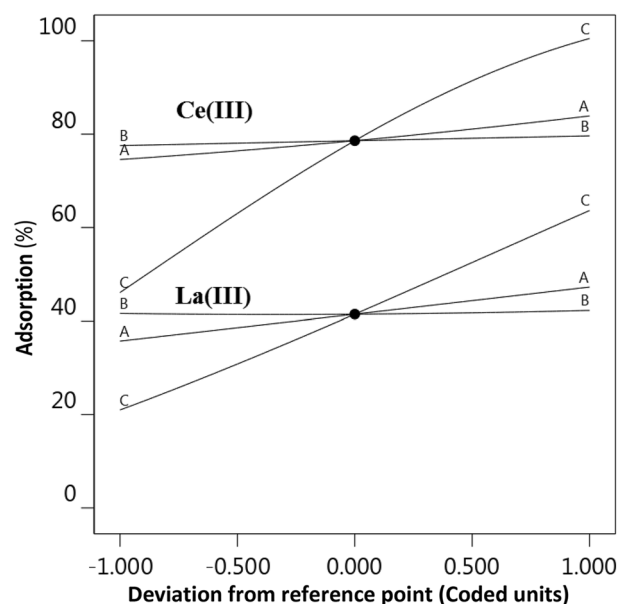


Figure 6. Perturbation plot for Ce(III) and La(III) ions adsorption models.

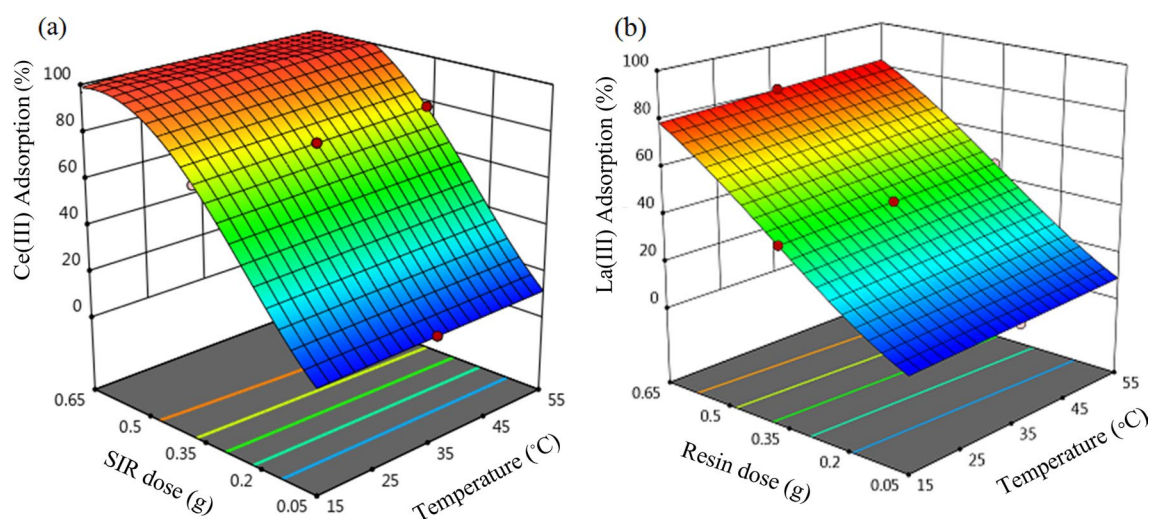


Figure 7. 3D sketches of the combined impact of temperature and SIR dose on the percentage adsorption of (a) Ce(III) and (b) La(III) (primary metal ions concentration 200 mg L⁻¹, pH = 4 and time 180 min).

Reliability of the experimental models. To achieve optimum conditions for the highest percentage adsorption of Ce(III) and La(III) ions on SIR, the optimization process was performed using response surface methodology. For this purpose, the optimization goal was set on the maximum percentage adsorption of Ce(III) and La(III) ions using minimum SIR amount in the investigated primary solution pH and temperature range. The experimental situations which provided the highest desirability (pH 6, 0.45 g SIR, and 25 °C adsorption temperature) were nominated as the optimum condition and need to be verified. The predicted and experimental results of Ce(III) and La(III) ions percentage adsorption are presented in Table 6. According to the results, the attained experimental data were compatible with the estimated results from the models, with somewhat minor error quantities (< 1%).

Investigating the adsorption kinetics. Investigation of adsorption kinetics is very useful for modeling the adsorption process and gives data regarding the adsorption mechanism and the transfer mode of solutes from the aqueous phase to the solid phase. The Ce(III) and La(III) adsorption kinetics were studied in the range of 5–240 min at a temperature of 25 °C, pH 6, the primary concentration of 200 mg L⁻¹, and SIR dose of 0.35 g. The obtained experimental result was examined by means of pseudo-first-order, the pseudo-second-order, and (IDMs) in their nonlinear form.

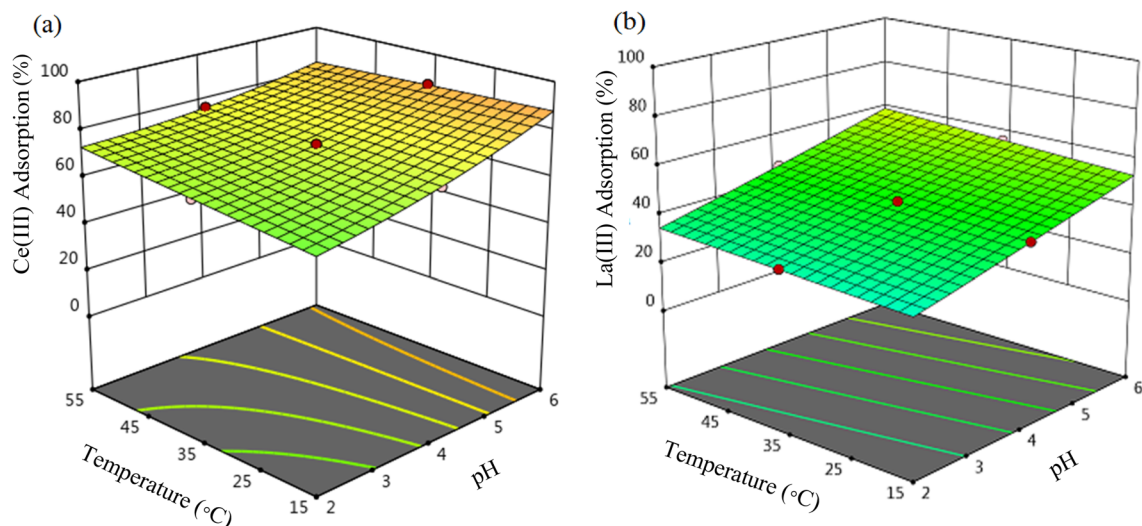


Figure 8. 3D figures of the combined impact of pH and temperature on the percentage adsorption of (a) Ce(III) and (b) La(III) (primary metal ions concentration 200 mg L⁻¹, SIR dose = 0.35 g and time 180 min).

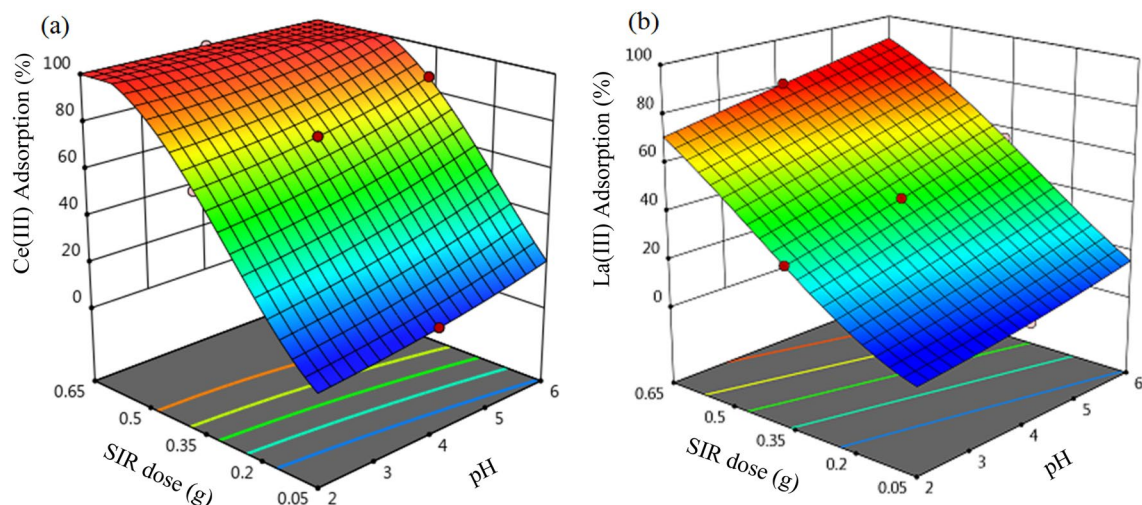


Figure 9. 3D curves of the combined effect of pH and SIR dose on the percentage adsorption of (a) Ce(III) and (b) La(III) (primary metal ions concentration 200 mg L⁻¹, temperature = 35 °C and time 180 min).

Metal ion	pH	Temperature (°C)	SIR dose (g)	Experimental	Predicted	Error %
Ce(III)	6	25	0.45	99.75	100	0.25
La(III)	6	25	0.45	69.98	70.67	0.98

Table 6. The optimum condition derived from RSM for Ce(III) and La(III) ions adsorption.

The nonlinear procedure of pseudo-first-order, pseudo-second-order, and (IDMs) are expressed by Eqs. (9), (10) and (11), respectively.

$$q_t = (q_e - e^{-k_1 t}) \tag{9}$$

$$q_t = \frac{k_2 q_e^2 t}{1 + k_2 q_e t} \tag{10}$$

$$q_t = k_{id}t^{1/2} + c \quad (11)$$

In these equations, q_e (mg g^{-1}) is the adsorption capacity at equilibrium, and q_t (mg g^{-1}) is the adsorption capacity at time t (min). The k_1 (min^{-1}) and k_2 ($\text{g mg}^{-1} \text{min}^{-1}$) are the pseudo-first-order and pseudo-second-order equation rate constants, correspondingly. In Eq. (8), K_p ($\text{mg g}^{-1} \text{min}^{-0.5}$) and C denote the intraparticle diffusion rate constant and thickness of the boundary layer, respectively^{68–71}.

The results of nonlinear kinetic data fitting for Ce(III) and La(III) ions adsorption on SIR are presented in Table 7. The amount of the kinetic models that matched the experimental results are evaluated using several error functions i.e. residual sum of squares error (SSE), coefficient of determination (R^2), root mean square error (RMSE), nonlinear chi-square (χ^2), and hybrid fractional error function (HYBRID). According to the reported results, the pseudo second-order kinetic model is well fitted to the experimental Ce(III) and La(III) ions adsorption data. This model relies on the supposition that chemisorption may be the rate-controlling step of the adsorption process and the Ce(III) and La(III) ions attached to the resin surface forms a chemical (in general covalent) bond and tends to find sites that make the coordination number the greatest possible with the surface^{72–76}.

According to the data depicted in Fig. 10, the adsorption capacity of Ce(III) and La(III) increased with rising contact time from 5 to 180 min and then remained constant due to the accumulation of Ce(III) and La(III) in the active sites on the SIR. Studies show that most of the adsorption process occurs in the first 80 min, which is due to the occupation of available resin surface sites for the adsorption of Ce(III) and La(III) ions. After all the foreign active sites on the SIR were saturated, the adsorption process slowed down to equilibrium. The reason for this is the low rate of saturation of the internal active sites of the adsorbent by metal ions and after 180 min the adsorption process reaches equilibrium.

Pseudo first order	Values		Pseudo second order	Values		Intraparticle diffusion	Values	
	Ce(III)	La(III)		Ce(III)	La(III)		Ce(III)	La(III)
q_e (mg g^{-1})	10.068	6.292	q_e (mg g^{-1})	11.829	7.935	K_{id} ($\text{mg g}^{-1} \text{min}^{-0.5}$)	0.659	0.456
k_1 (min^{-1})	0.024	0.015	k_2 ($\text{g mg}^{-1} \text{min}^{-1}$)	0.0028	0.0017	C	1.621	-0.083
R^2	0.977	0.986	R^2	0.993	0.994	R^2	0.855	0.962
SSE	1.744	0.373	SSE	0.512	0.209	SSE	11.120	1.240
χ^2	0.385	0.163	χ^2	0.192	0.048	χ^2	2.122	0.354
RMSE	0.467	0.216	RMSE	0.253	0.162	RMSE	1.179	0.394
HYBRID	-9.116	-11.383	HYBRID	-0.055	-0.227	HYBRID	0.441	-0.105

Table 7. Parameters of kinetic models for Ce(III) and La(III) Adsorption onto SIR ([Ce-La] = 200 mg/L, pH = 5, SIR dose = 0.4 g, Stirring speed = 200 rpm, and temperature = 25 ± 2 °C).

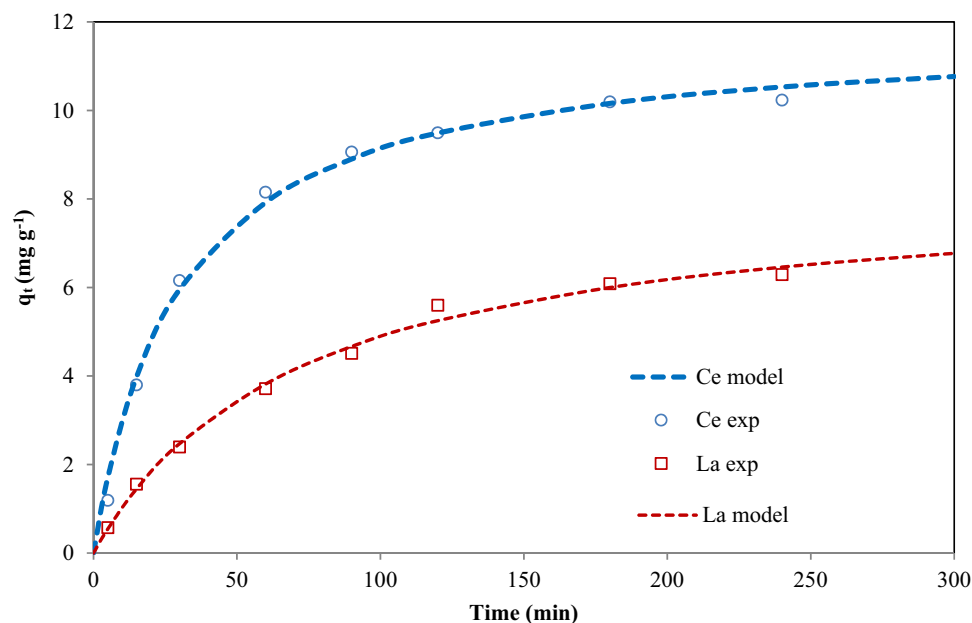


Figure 10. Nonlinear fit of the pseudo-second order kinetic model of Ce(III) and La(III) ions adsorption onto SIR ([Ce-La] = 200 mg/L, pH = 5, SIR dose = 0.4 g, Stirring velocity = 200 rpm, and temperature = 25 ± 2 °C).

The equilibrium adsorption capacity (q_e) is found to be 11.829 mg g⁻¹ and 7.935 mg g⁻¹ for Ce(III) and La(III) ions, correspondingly. The rate constant of PSO equation (k_2) of 0.0028 and 0.0017 g mg⁻¹ min⁻¹ is calculated for Ce(III) and La(III) ions, respectively. These results demonstrate that the PSO adsorption mechanism is overriding and the rate of each ion is controlled by the chemisorption process.

Investigating the adsorption isotherms. Adsorption isotherms are mathematical relationships that aim to establish a quantitative correlation between the value of matter adsorbed on a solid surface and its concentration in the liquid phase. Equilibrium adsorption isotherm provides important information about the adsorption mechanism. In this study, 6 isotherms patterns of Langmuir, Freundlich, Temkin, and Sips were employed in nonlinear form for analyzing the Ce(III) and La(III) ions adsorption on SIR in the concentration limit of 50 to 250 mg L⁻¹. The nonlinear type of Freundlich, Langmuir, Temkin, and sips isotherm models are expressed by Eqs. (12)–(15), correspondingly.

$$q_e = k_f C_e^{1/n} \quad (12)$$

$$q_e = \frac{q_m k_L C_e}{1 + k_L C_e} \quad (13)$$

$$q_e = \frac{RT}{b_T} \ln(A_T C_e) \quad (14)$$

$$q_e = \frac{q_m K_S C_e^{m_S}}{1 + K_S C_e^{m_S}} \quad (15)$$

where C_e is the metal ions equilibrium concentration (mg L⁻¹), and q_e is the equilibrium adsorption value (mg g⁻¹).

In the Freundlich equation, k_f signifies the adsorbent capacity (L g⁻¹), and n reflects the intensity of the adsorption.

In the Langmuir isotherm pattern, q_m is the maximum adsorption capacity (mg g⁻¹), and K_L signifies the Langmuir constant (L mg⁻¹).

In Temkin isotherm, $B_T = \frac{RT}{b_T}$ is the Temkin constant, and A_T is the equilibrium binding constant (L g⁻¹).

In the Sips isotherm model, q_{ms} is the Sips maximum adsorption capacity (mg g⁻¹) and K_S is the equilibrium constant (L mg⁻¹), and m_S is the Sips model exponent.

The parameters of the investigated isotherm models for Ce(III) and La(III) adsorption onto SIR were acquired using nonlinear least-squares fitting of the experimental data and presented in Table 8. The quality of investigated isotherm models was evaluated using previously mentioned error functions^{77,78}.

According to the obtained data, the Sips isotherm was the best fitting isotherm model for evaluating Ce(III) and La(III) ions adsorption onto SIR. The maximum adsorption capacity obtained for Ce(III) and La(III) ions were 11.873 and 6.324 mg g⁻¹, respectively.

The 3-parameter Sips isotherm pattern is an association of Langmuir and Freundlich two-parameter patterns and therefore it could theoretically offer better calculations for equilibrium results than these two isotherm

Langmuir	Ce(III)	La(III)	Freundlich	Ce(III)	La(III)
q_m (mg g ⁻¹)	10.489	6.2436	K_f (mg g ⁻¹)(L mg ⁻¹) ⁻ⁿ	5.588	4.174
K_L (L mg ⁻¹)	1.854	5.063	n	5.533	10.532
R^2	0.972	0.988	R^2	0.936	0.801
SSE	1.630	0.121	SSE	2.969	1.873
χ^2	0.517	0.020	χ^2	0.532	0.454
RMSE	0.571	0.155	RMSE	0.771	0.612
HYBRID	-14.080	-0.413	HYBRID	4.798	1.559
Temkin	Ce(III)	La(III)	Sips	Ce(III)	La(III)
$\frac{1}{b_T}$ (J mol ⁻¹)	5.453E-04	2.028E-04	q_m (mg g ⁻¹)	11.873	7.324
A_T	79.146	4248.859	K_S (Lmg ⁻¹) ^{m_S}	1.056	3.590
			m_S	0.577	0.818
R^2	0.989	0.866	R^2	0.998	0.993
SSE	0.545	1.336	SSE	0.100	0.071
χ^2	0.078	0.314	χ^2	0.011	0.011
RMSE	0.330	0.517	RMSE	0.141	0.119
HYBRID	1.343	0.911	HYBRID	0.697	0.046

Table 8. Isotherm models' factors and assessed quantities for Ce(III) and La(III) adsorption onto SIR (pH=5, SIR dose=0.4 g, stirring speed=200 rpm, contact time=180 min, and temperature=25±2 °C).

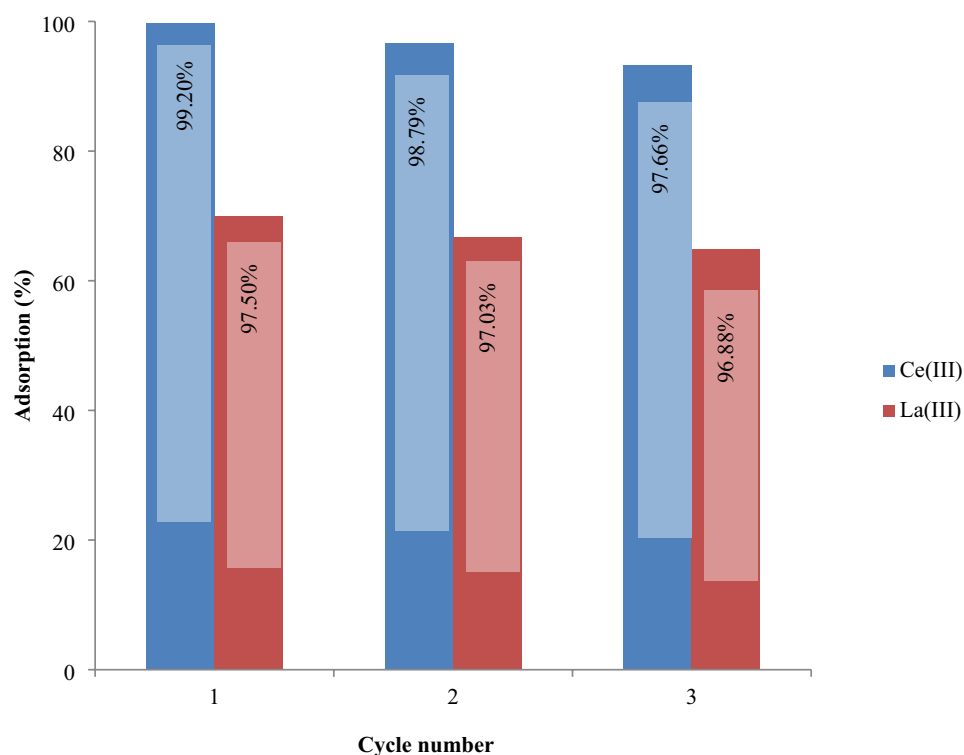


Figure 11. Adsorption–Desorption efficiency of SIR in 3 consecutive cycles using HCL 0.1 mol L⁻¹.

models. The Sips isotherm model showed the monolayer adsorption of one adsorbate molecule onto 1/n_s adsorption sites and is suitable for estimating the heterogeneous adsorption scheme. This model also overcomes the drawback associated with the Freundlich isotherm model when the concentration is satisfactorily high^{79,80}.

Investigating the desorption process. The literature review indicates that SIRs are efficiently employed for the extraction of metal ions with well stability during several adsorption–desorption cycles. In present work also, the used Amberlite XAD-7 resin impregnated via CYANEX-272 extractant was recovered 3 times and showed high stability during 3 adsorption–desorption cycles.

The desorption study on the SIR containing Ce(III) and La(III) ions was conducted using 0.1 M HCl solution and the data are illustrated in Fig. 11. As could be observed, the percentage adsorption of Ce(III) and La(III) ions onto SIR decreased from 99.75% and 69.98% in the first cycle to 93.22% and 64.85% in the third cycle, respectively. Furthermore, the efficiency of 0.1 M HCl in the desorption of Ce(III) and La(III) ions from SIR decreased from 99.20% and 97.50% in the first cycle to 97.66% and 96.88% in the third cycle, correspondingly. As could be observed, the Ce(III) and La(III) ions recovery values are over 96%. According to the obtained results, SIR could be reprocessed many times with no substantial reduction in metal ion adsorption percentage. Similar results have been obtained from other studies for the regeneration and metallic ions recovery for using impregnated Amberlite XAD7HP resin for As(V), Pb(II) and Cd(II) sorption⁸¹.

Conclusions

The current research work was performed to study the adsorption of Ce(III) and La(III) ions from an aqueous mixture through A XAD-7 resin impregnated with CYANEX-272 in the batch system. The prepared SIR was characterized using SEM-EDS, BET, and FTIR analysis techniques. The impact of three process-independent factors individual pH, Temperature, and SIR dose was scrutinized via RSM according to CCD. The Ce(III) and La(III) ions adsorption data were compatible to a second order polynomial model with the square root transform function. Based on the analysis of variance (ANOVA), the SIR dose was determined as the most effectual factor on Ce(III) and La(III) ions percentage adsorption. The equilibrium results were examined using the Langmuir, Freundlich, Temkin, and Sips sorption isotherm models. The data revealed the compromise of Ce(III) and La(III) ions adsorption onto SIR with the Sips isotherm model and the highest adsorption value obtained for Ce(III) and La(III) ions were 11.873 and 6.324 mg g⁻¹, correspondingly. The kinetic studies were conducted using the pseudo-first-order, the pseudo-second-order, and (IDMs). based on the data obtained, kinetic data were fitted satisfactory to a pseudo-second-order rate correlation. The adsorption/desorption study was also performed for 3 cycles and the data revealed that the SIR could be reused several times for Ce(III) and La(III) ions adsorption without a significant performance decrement. According to the results, AXAD-7 resin impregnated with CYANEX-272 can be effectively used for Ce(III) and La(III) ions adsorption from aqueous solutions.

Data availability

The datasets used and/or analyzed during the current study are available from the corresponding author on reasonable request.

Received: 9 February 2023; Accepted: 25 April 2023

Published online: 28 April 2023

References

- Mondal, S. *et al.* Recovery of rare earth elements from coal fly ash using TEHDGA impregnated resin. *Hydrometallurgy* **185**, 93–101 (2019).
- Khani, M. Biosorption of strontium by *Padina* sp. algae biomass: Process optimisation and equilibrium study. *Int. J. Environ. Technol. Manag.* **16**, 290–311 (2013).
- Liu, W. *et al.* Treatment of Cr^{VI}-containing Mg(OH)₂ nanowaste. *Angew. Chem.* **120**, 5701–5704 (2008).
- Wang, Y. *et al.* Non-free Fe dominated PMS activation for enhancing electro-Fenton efficiency in neutral wastewater. *J. Electroanal. Chem.* **928**, 117062 (2023).
- Atwood, D. A. *The Rare Earth Elements: Fundamentals and Applications* (John Wiley & Sons, 2013).
- Ahmadi-Motlagh, M., Amini, Y. & Karimi-Sabet, J. Experimental study of nitrogen isotope separation by ion-exchange chromatography: Effect of process factors. *J. Radioanal. Nucl. Chem.* **331**, 309–315 (2022).
- Zhang, L. *et al.* The effect of pH/PAC on the coagulation of anionic surfactant wastewater generated in the cosmetic production. *J. Environ. Chem. Eng.* **11**, 109312 (2023).
- Wang, Z., Liu, X., Ni, S.-Q., Zhuang, X. & Lee, T. Nano zero-valent iron improves anammox activity by promoting the activity of quorum sensing system. *Water Res.* **202**, 117491 (2021).
- Braun, J.-J., Pagel, M., Herbillin, A. & Rosin, C. Mobilization and redistribution of REEs and thorium in a syenitic lateritic profile: A mass balance study. *Geochim. Cosmochim. Acta* **57**, 4419–4434 (1993).
- Khani, M. H. Statistical analysis and isotherm study of uranium biosorption by *Padina* sp. algae biomass. *Environ. Sci. Pollut. Res.* **18**, 790–799 (2011).
- Jowitt, S. M., Werner, T. T., Weng, Z. & Mudd, G. M. Recycling of the rare earth elements. *Curr. Opin. Green Sustain. Chem.* **13**, 1–7 (2018).
- Khani, M., Keshtkar, A., Ghannadi, M. & Pahlavanzadeh, H. Equilibrium, kinetic and thermodynamic study of the biosorption of uranium onto *Cystoseria indica* algae. *J. Hazard. Mater.* **150**, 612–618 (2008).
- Gupta, C. K. & Krishnamurthy, N. Extractive metallurgy of rare earths. *Int. Mater. Rev.* **37**, 197–248 (1992).
- Ghorbanpour Khamesh, A. A., Amini, Y., Shademan, M. M. & Ghazanfari, V. Intensification of thorium biosorption onto protonated orange peel using the response surface methodology. *Chem. Prod. Process Model.* <https://doi.org/10.1515/cppm-2022-0085> (2023).
- Bai, B., Bai, F., Sun, C., Nie, Q. & Sun, S. Adsorption mechanism of shell powders on heavy metal ions Pb²⁺/Cd²⁺ and the purification efficiency for contaminated soils. *Front. Earth Sci.* **10**, 1071228 (2023).
- Zhang, X. *et al.* Plutonium reactive transport in fractured granite: Multi-species experiments and simulations. *Water Res.* **224**, 119068 (2022).
- Nishihama, S., Kohata, K. & Yoshizuka, K. Separation of lanthanum and cerium using a coated solvent-impregnated resin. *Sep. Purif. Technol.* **118**, 511–518 (2013).
- Keshtkar, A. R., Moosavian, M. A., Sohbatzadeh, H. & Mofras, M. La (III) and Ce (III) biosorption on sulfur functionalized marine brown algae *Cystoseria indica* by xanthation method: Response surface methodology, isotherm and kinetic study. *Groundw. Sustain. Dev.* **8**, 144–155 (2019).
- Aguilar, M. & Cortina, J. L. *Solvent Extraction and Liquid Membranes: Fundamentals and Applications in New Materials* (CRC Press, 2008).
- Van Nguyen, N., Iizuka, A., Shibata, E. & Nakamura, T. Study of adsorption behavior of a new synthesized resin containing glycolic amic acid group for separation of scandium from aqueous solutions. *Hydrometallurgy* **165**, 51–56 (2016).
- Jia, Q., Wang, Z., Li, D. & Niu, C. Adsorption of heavy rare earth (III) with extraction resin containing bis (2, 4, 4-trimethylpentyl) mono thiophosphinic acid. *J. Alloys Compd.* **374**, 434–437 (2004).
- Sert, Ş *et al.* Investigation of sorption behaviors of La, Pr, Nd, Sm, Eu and Gd on D2EHPA-impregnated XAD7 resin in nitric acid medium. *Sep. Sci. Technol.* **56**, 26–35 (2021).
- Kammerer, D. R., Kammerer, J. & Carle, R. in *Polyphenols in Plants* 327–339 (Elsevier, 2019).
- Nguyen, T. H. & Lee, M. S. A review on separation of gallium and indium from leach liquors by solvent extraction and ion exchange. *Min. Process. Extr. Metall. Rev.* <https://doi.org/10.1080/08827508.2018.1538987> (2018).
- Moyer, B. A. *Ion Exchange and Solvent Extraction: A Series of Advances* Vol. 19 (CRC Press, 2009).
- Navarro, R., Gallardo, V., Saucedo, I. & Guibal, E. Extraction of Fe (III) from hydrochloric acid solutions using Amberlite XAD-7 resin impregnated with trioctylphosphine oxide (Cyanex 921). *Hydrometallurgy* **98**, 257–266 (2009).
- Kabay, N., Cortina, J. L., Trochimczuk, A. & Streat, M. Solvent-impregnated resins (SIRs)—methods of preparation and their applications. *React. Funct. Polym.* **70**, 484–496 (2010).
- Masry, B., Abu Elgoud, E. & Rizk, S. Modeling and equilibrium studies on the recovery of praseodymium (III), dysprosium (III) and yttrium (III) using acidic cation exchange resin. *BMC Chemistry* **16**, 37 (2022).
- Masry, B. A. & Daoud, J. A. Sorption behavior of tungsten and molybdenum on TVEX-TOPO resin from nitric acid solution. *J. Chem. Technol. Biotechnol.* **96**, 1399–1410 (2021).
- Noweir, H., Masry, B., Zeid, M., Kassem, A. & Daoud, J. Sorption of Mo (VI) from nitric acid solution using SM-4 copolymer resin impregnated with CYANEX 923. *J. Inorg. Organomet. Polym. Mater.* **31**, 1576–1589 (2021).
- Draa, M., Belaid, T. & Benamor, M. Extraction of Pb (II) by XAD7 impregnated resins with organophosphorus extractants (DEHPA, IONQUEST 801, CYANEX 272). *Sep. Purif. Technol.* **40**, 77–86 (2004).
- El-Sofany, E. Removal of lanthanum and gadolinium from nitrate medium using Aliquat-336 impregnated onto Amberlite XAD-4. *J. Hazard. Mater.* **153**, 948–954 (2008).
- Belkhouche, N.-E. & Didi, M. A. Extraction of Bi (III) from nitrate medium by D2EHPA impregnated onto Amberlite XAD-1180. *Hydrometallurgy* **103**, 60–67 (2010).
- Fouad, H., Abu Elenein, S., Orabi, A. & Abdumoteleb, S. A new extractant impregnated resin for separation of traces of uranium and thorium followed by their spectrophotometric determination in some geological samples. *SN Appl. Sci.* **1**, 1–18 (2019).
- Liao, C.-F., Jiao, Y.-F., Liang, Y., Jiang, P.-G. & Nie, H.-P. Adsorption-extraction mechanism of heavy rare earth by Cyanex272-P507 impregnated resin. *Trans. Nonferrous Met. Soc. China* **20**, 1511–1516 (2010).
- Benamor, M., Bouariche, Z., Belaid, T. & Draa, M. Kinetic studies on cadmium ions by Amberlite XAD7 impregnated resins containing di (2-ethylhexyl) phosphoric acid as extractant. *Sep. Purif. Technol.* **59**, 74–84 (2008).
- Chen, J. H., Kao, Y. Y. & Lin, C. H. Selective separation of vanadium from molybdenum using D2EHPA-immobilized Amberlite XAD-4 Resin. *Sep. Sci. Technol.* **38**, 3827–3852 (2003).

38. El Didamony, A., Youssef, W. & Abdou, A. Modification of Amberlite XAD-2 resin for U (VI) adsorption from Egyptian crude phosphoric acid. *Egypt. J. Pet.* **28**, 71–76 (2019).
39. Batra, S., Datta, D., Beesabathuni, N. S., Kanjolia, N. & Saha, S. Adsorption of Bisphenol-A from aqueous solution using amberlite XAD-7 impregnated with aliquat 336: Batch, column, and design studies. *Process Saf. Environ. Prot.* **122**, 232–246 (2019).
40. Kalal, H. S. *et al.* The adsorption-desorption behavior of strontium ions with an impregnated resin containing di (2-ethylhexyl) phosphoric acid in aqueous solutions. *Adv. Environ. Res.* **6**, 301–315 (2017).
41. Lin, X. *et al.* Membrane inlet mass spectrometry method (REOX/MIMS) to measure 15N-nitrate in isotope-enrichment experiments. *Ecol. Ind.* **126**, 107639 (2021).
42. Liang, Y. *et al.* Benzene decomposition by non-thermal plasma: A detailed mechanism study by synchrotron radiation photoionization mass spectrometry and theoretical calculations. *J. Hazard. Mater.* **420**, 126584 (2021).
43. Cheng, C., Yang, X., Jiang, F. & Yang, Z. How to synergize different institutional logics of firms in cross-border acquisitions: A matching theory perspective. *Manag. Int. Rev.* <https://doi.org/10.1007/s11575-023-00502-8> (2023).
44. Dong, P. *et al.* First-principles study on the adsorption characteristics of corrosive species on passive film TiO₂ in a NaCl solution containing H₂S and CO₂. *Metals* **12**, 1160 (2022).
45. Cheng, M. *et al.* Effect of dual-modified cassava starches on intelligent packaging films containing red cabbage extracts. *Food Hydrocoll.* **124**, 107225 (2022).
46. Kalavathy, H., Regupathi, I., Pillai, M. G. & Miranda, L. R. Modelling, analysis and optimization of adsorption parameters for H₃PO₄ activated rubber wood sawdust using response surface methodology (RSM). *Colloids Surf. B* **70**, 35–45 (2009).
47. Amini, Y. *et al.* Optimization of liquid-liquid extraction of calcium with a serpentine microfluidic device. *Int. Commun. Heat Mass Transf.* **140**, 106551 (2023).
48. Abdollahi, P., Karimi-Sabet, J., Moosavian, M. A. & Amini, Y. Microfluidic solvent extraction of calcium: Modeling and optimization of the process variables. *Sep. Purif. Technol.* **231**, 115875 (2020).
49. Marsousi, S., Karimi-Sabet, J., Moosavian, M. A. & Amini, Y. Liquid-liquid extraction of calcium using ionic liquids in spiral microfluidics. *Chem. Eng. J.* **356**, 492–505 (2019).
50. Jahromi, P. F., Karimi-Sabet, J. & Amini, Y. Ion-pair extraction-reaction of calcium using Y-shaped microfluidic junctions: An optimized separation approach. *Chem. Eng. J.* **334**, 2603–2615 (2018).
51. Hashemipour, N. *et al.* Experimental and simulation investigation on separation of binary hydrocarbon mixture by thermogravimational column. *J. Mol. Liq.* **268**, 791–806 (2018).
52. Jahromi, P. F., Karimi-Sabet, J., Amini, Y. & Fadaei, H. Pressure-driven liquid-liquid separation in Y-shaped microfluidic junctions. *Chem. Eng. J.* **328**, 1075–1086 (2017).
53. Ahmad, J. *et al.* Insight into single-element nobel metal anisotropic silver nanoparticle shape-dependent selective ROS generation and quantification. *RSC Adv.* **11**, 8314–8322 (2021).
54. Tang, F., Wang, H., Chang, X.-H., Zhang, L. & Alharbi, K. H. Dynamic event-triggered control for discrete-time nonlinear Markov jump systems using policy iteration-based adaptive dynamic programming. *Nonlinear Anal. Hybrid Syst.* **49**, 101338 (2023).
55. Yang, X.-Y. *et al.* Solvent impregnated resin prepared using ionic liquid Cyphos IL 104 for Cr (VI) removal. *Trans. Nonferrous Met. Soc. China* **22**, 3126–3130 (2012).
56. Mihăilescu, M. *et al.* Gold (III) adsorption from dilute waste solutions onto Amberlite XAD7 resin modified with L-glutamic acid. *Sci. Rep.* **9**, 1–13 (2019).
57. İnan, S. *et al.* Extraction and separation studies of rare earth elements using Cyanex 272 impregnated Amberlite XAD-7 resin. *Hydrometallurgy* **181**, 156–163 (2018).
58. Mosleh, S., Rahimi, M., Ghaedi, M., Dashtian, K. & Hajati, S. BiPO₄/Bi₂S₃-HKUST-1-MOF as a novel blue light-driven photocatalyst for simultaneous degradation of toluidine blue and auramine-O dyes in a new rotating packed bed reactor: Optimization and comparison to a conventional reactor. *RSC Adv.* **6**, 63667–63680 (2016).
59. Azad, F. N. *et al.* Preparation and characterization of MWCNTs functionalized by N-(3-nitrobenzylidene)-N'-trimethoxysilylpropyl-ethane-1, 2-diamine for the removal of aluminum (iii) ions via complexation with eriochrome cyanine R: Spectrophotometric detection and optimization. *RSC Adv.* **5**, 61060–61069 (2015).
60. Zhang, H., Wang, H., Niu, B., Zhang, L. & Ahmad, A. M. Sliding-mode surface-based adaptive actor-critic optimal control for switched nonlinear systems with average dwell time. *Inf. Sci.* **580**, 756–774 (2021).
61. Cheng, Y., Niu, B., Zhao, X., Zong, G. & Ahmad, A. M. Event-triggered adaptive decentralised control of interconnected nonlinear systems with Bouc-Wen hysteresis input. *Int. J. Syst. Sci.* <https://doi.org/10.1080/00207721.2023.2169845> (2023).
62. Li, P., Yang, M. & Wu, Q. Confidence interval based distributionally robust real-time economic dispatch approach considering wind power accommodation risk. *IEEE Trans. Sustain. Energy* **12**, 58–69 (2020).
63. Şahan, T. Application of RSM for Pb (II) and Cu (II) adsorption by bentonite enriched with SH groups and a binary system study. *J. Water Process Eng.* **31**, 100867 (2019).
64. Marin, N. M., Fical, A., Constantin, L. A., Motelica, L. & Trusca, R. New chelate resins prepared with direct red 23 for Cd²⁺, Ni²⁺, Cu²⁺ and Pb²⁺ removal. *Polymers* **14**, 5523 (2022).
65. Scholes, F., Soste, C., Hughes, A., Hardin, S. & Curtis, P. The role of hydrogen peroxide in the deposition of cerium-based conversion coatings. *Appl. Surf. Sci.* **253**, 1770–1780 (2006).
66. Borai, E. H., El-Din, A. M. S., El-Sofany, E. A., Sakr, A. A. & El-Sayed, G. O. Electrochemical generation of hydrogen peroxide for oxidation and separation of trivalent cerium in acidic medium.
67. Suzuki, Y., Nagayama, T., Sekine, M., Mizuno, A. & Yamaguchi, K. Precipitation incidence of the lanthanoid (III) hydroxides. *J. Less Common Met.* **126**, 351–356 (1986).
68. Xue, B. *et al.* Kinetics of mixed rare earths minerals decomposed by CaO with NaCl-CaCl₂ melting salt. *J. Rare Earths* **28**, 86–90 (2010).
69. Kumari, A., Sinha, M. K., Pramanik, S. & Sahu, S. K. Recovery of rare earths from spent NdFeB magnets of wind turbine: Leaching and kinetic aspects. *Waste Manag.* **75**, 486–498 (2018).
70. Si, Z., Yang, M., Yu, Y. & Ding, T. Photovoltaic power forecast based on satellite images considering effects of solar position. *Appl. Energy* **302**, 117514 (2021).
71. Tan, J. *et al.* Screening of endocrine disrupting potential of surface waters via an affinity-based biosensor in a rural community in the Yellow River Basin, China. *Environ. Sci. Technol.* **56**, 14350–14360 (2022).
72. Atkins, P. & De Paula, J. *Elements of Physical Chemistry* (Oxford University Press, 2013).
73. Robati, D. Pseudo-second-order kinetic equations for modeling adsorption systems for removal of lead ions using multi-walled carbon nanotube. *J. Nanostruct. Chem.* **3**, 1–6 (2013).
74. Wang, M., Yang, M., Fang, Z., Wang, M. & Wu, Q. A practical feeder planning model for urban distribution system. *IEEE Trans. Power Syst.* <https://doi.org/10.1109/TPWRS.2022.3170933> (2022).
75. Li, Y., Wang, H., Zhao, X. & Xu, N. Event-triggered adaptive tracking control for uncertain fractional-order nonstrict-feedback nonlinear systems via command filtering. *Int. J. Robust Nonlinear Control* **32**, 7987–8011 (2022).
76. Cheng, F., Liang, H., Niu, B., Zhao, N. & Zhao, X. Adaptive neural self-triggered bipartite secure control for nonlinear MASs subject to DoS attacks. *Inf. Sci.* <https://doi.org/10.1016/j.ins.2023.02.058> (2023).
77. Herald, E., Hidayat, Y. & Firdaus, M. in *IOP Conference Series: Materials science and engineering* 012067 (IOP Publishing).

78. Rostamian, R., Najafi, M. & Rafati, A. A. Synthesis and characterization of thiol-functionalized silica nano hollow sphere as a novel adsorbent for removal of poisonous heavy metal ions from water: Kinetics, isotherms and error analysis. *Chem. Eng. J.* **171**, 1004–1011 (2011).
79. Ho, Y., Porter, J. & McKay, G. Equilibrium isotherm studies for the sorption of divalent metal ions onto peat: Copper, nickel and lead single component systems. *Water Air Soil Pollut.* **141**, 1–33 (2002).
80. Eftekhari, M. *et al.* Cadmium and copper heavy metal treatment from water resources by high-performance folic acid-graphene oxide nanocomposite adsorbent and evaluation of adsorptive mechanism using computational intelligence, isotherm, kinetic, and thermodynamic analyses. *Environ. Sci. Pollut. Res.* **27**, 43999–44021 (2020).
81. Marin, N. M. & Stanculescu, I. Removal of procainamide and lidocaine on Amberlite XAD7HP resin and of As (V), Pb (II) and Cd (II) on the impregnated resin for water treatment. *Mater. Chem. Phys.* **277**, 125582 (2022).

Author contributions

A.Y.: wrote the main manuscript text, prepared figures and tables, reviewed the manuscript. M.N.Z.: wrote the main manuscript text, prepared figures and tables. M.H.K.: wrote the main manuscript text, prepared figures. Y.A.: wrote the main manuscript text, prepared tables, reviewed the manuscript.

Funding

This research did not receive any specific grant from funding agencies in the public, commercial, or not-for-profit sectors.

Competing interests


The authors declare no competing interests.

Additional information

Correspondence and requests for materials should be addressed to M.H.K. or Y.a.

Reprints and permissions information is available at www.nature.com/reprints.

Publisher's note Springer Nature remains neutral with regard to jurisdictional claims in published maps and institutional affiliations.

 **Open Access** This article is licensed under a Creative Commons Attribution 4.0 International License, which permits use, sharing, adaptation, distribution and reproduction in any medium or format, as long as you give appropriate credit to the original author(s) and the source, provide a link to the Creative Commons licence, and indicate if changes were made. The images or other third party material in this article are included in the article's Creative Commons licence, unless indicated otherwise in a credit line to the material. If material is not included in the article's Creative Commons licence and your intended use is not permitted by statutory regulation or exceeds the permitted use, you will need to obtain permission directly from the copyright holder. To view a copy of this licence, visit <http://creativecommons.org/licenses/by/4.0/>.

© The Author(s) 2023